

Biochemical characteristics of the 6-nitro regioisomer of nitroxoline and its 1,2,3,4-tetrahydroquinoline analogs

ANA MITROVIĆ^{1,2}

DAMIJAN KNEZ¹

MARTINA HRAST RAMBAHER¹

JAKOB KLJUN³

JANKO KOS^{1,2}

STANISLAV GOBEC¹

IZIDOR SOSIČ^{1,*}

¹ *Faculty of Pharmacy, University of Ljubljana, 1000 Ljubljana, Slovenia*

² *Department of Biotechnology, Jožef Stefan Institute, 1000 Ljubljana, Slovenia*

³ *Faculty of Chemistry and Chemical Technology, University of Ljubljana, 1000 Ljubljana, Slovenia*

Correspondence; e-mail: izidor.sosic@ffa.uni-lj.si

ORCID*s*:

ANA MITROVIĆ^{1,2} [0000-0002-6996-4831](https://orcid.org/0000-0002-6996-4831)

DAMIJAN KNEZ¹ [0000-0001-9917-1384](https://orcid.org/0000-0001-9917-1384)

MARTINA HRAST RAMBAHER¹ [0000-0003-0488-2445](https://orcid.org/0000-0003-0488-2445)

JAKOB KLJUN³ [0000-0002-1986-4840](https://orcid.org/0000-0002-1986-4840)

JANKO KOS^{1,2} [0000-0002-4228-3518](#)

STANISLAV GOBEC [0000-0002-9678-3083](#)

IZIDOR SOSIČ 0000-0002-3370-4587

ABSTRACT

Significant amount of data about the different pharmacological activities of established antimicrobial compound nitroxoline (8-hydroxy-5-nitroquinoline) is available in the scientific literature. On the other hand, its regioisomer 8-hydroxy-6-nitroquinoline was never characterized biochemically and the same also applies to their 1,2,3,4-tetrahydroquinoline analogs. Herein, we determined the influence of pyridine ring saturation and the position of the nitro group on various biochemical characteristics of compounds, such as metal-chelating properties, inhibition of methionine aminopeptidases (MetAPs) from *Mycobacterium tuberculosis* and human MetAP2, as well as antibacterial activities on *Escherichia coli*, *Staphylococcus aureus*, and *Mycobacterium smegmatis*. In addition, inhibition of endopeptidase and exopeptidase activities of cathepsin B was determined, together with the ability of new nitroxoline analogs to reduce intracellular collagen IV degradation. Substantially different biological activities were observed for the 6-nitro regioisomer of nitroxoline, as well as for both of their partially saturated counterparts.

Keywords: 8-hydroxyquinoline, 1,2,3,4-tetrahydroquinoline, regioisomer, antibacterial activity, cathepsin B, methionine aminopeptidase

Accepted May 30, 2025

Published online June 1, 2025

INTRODUCTION

Nitroxoline (8-hydroxy-5-nitroquinoline) has been a marketed drug for more than 50 years and is currently used for the treatment of urinary tract infections (1). It does not belong to any class of antimicrobial drugs and it appears that its mechanism of action primarily involves the binding of essential metal cations, which are crucial for microbial growth (2–4). Namely, nitroxoline effectively chelates bivalent metal cations such as Mg^{2+} , Mn^{2+} , Fe^{2+} , and Zn^{2+} (2, 5). This chelation is vital for its bacteriostatic activity, as it deprives bacteria of these essential micronutrients needed for growth. Nitroxoline has potent antibacterial effects against most Gram-positive and Gram-negative uropathogenic bacteria (1, 6, 7), including *Acinetobacter baumannii* (8) and *Klebsiella pneumoniae* (9). Nitroxoline also demonstrates antibacterial activity against *Mycobacterium bovis* BCG with an MIC value of $10\ \mu\text{mol L}^{-1}$ (3) and recent studies showed its excellent potential against 18 clinical isolates of *Mycobacterium tuberculosis* (*M. tuberculosis*) complex *in vitro* (10). In addition, because of its ability to chelate Zn^{2+} and Fe^{2+} from the biofilm matrix, nitroxoline can also inhibit bacterial biofilm formation and cause a reduction in bacterial adhesion to uroepithelial cells (1, 11). Recently, it was also demonstrated that nitroxoline potently inhibits New Delhi metallo- β -lactamase, most probably *via* stripping the Zn^{2+} ions from its catalytic center (12).

Beyond its antibacterial role, nitroxoline gained attention due to other biological activities, such as inhibition of cathepsin B (catB) (13), methionine aminopeptidase 2 (MetAP2) (14), sirtuin-1 (14), bromodomain-containing protein 4 (15), and disruption of Forkhead box protein M1 signaling (16). Several other independent studies also demonstrated that nitroxoline inhibits the proliferation of glioblastoma cells (17), and induces apoptosis in multiple myeloma cell lines (18) and prostate cancer cells (19, 20). Mechanistic details of anticancer activities are thoroughly described in a recent review (21).

Despite biological activities described for nitroxoline, we found it interesting that its regioisomer, *i.e.*, 8-hydroxy-6-nitroquinoline was never characterized biochemically. To the

best of our knowledge, the partially saturated analogs of either nitroxoline or the 6-nitro derivative were also never assayed for their biological activities. Moreover, we found no details on the synthetic preparation of partially saturated analogs. Herein, we report the synthesis and biological evaluation of 8-hydroxy-5-nitro-1,2,3,4-tetrahydroquinoline and 8-hydroxy-6-nitro-1,2,3,4-tetrahydroquinoline and compare their pharmacological activities with nitroxoline and 8-hydroxy-6-nitroquinoline (Fig. 1). The influence of partial saturation and the position of nitro group on pharmacological characteristics was tested in a variety of biochemical settings. Namely, we assayed all compounds for their ability to chelate divalent cations, to inhibit MetAP1a from *M. tuberculosis* and human MetAP2, to prevent bacterial growth, to inhibit endopeptidase and exopeptidase activities of cathepsin B, and for their ability to reduce intracellular collagen IV degradation. The results showed that biological activities of new derivatives were substantially different in comparison to nitroxoline. In most cases, pharmacological activities were diminished; however, some analogs proved to be better inhibitors of catB or of MetAPs compared to parent nitroxoline, thus representing valuable starting points for hit-to-lead optimization.

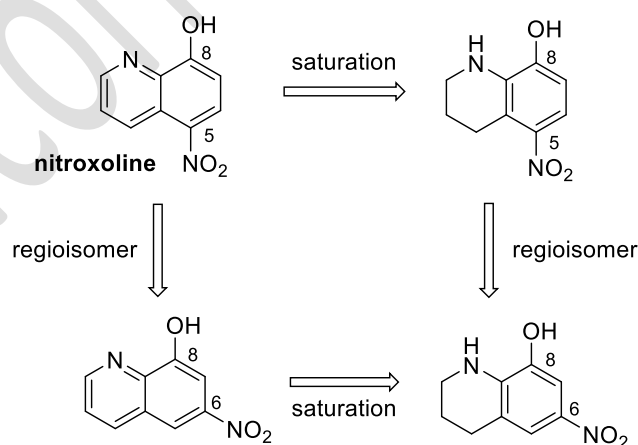


Fig. 1. Schematic representation of nitroxoline analogs prepared in this manuscript.

EXPERIMENTAL

General chemistry remarks

Chemicals from commercial sources (Sigma-Aldrich, Fluorochem, TCI, Apollo Scientific, Enamine) were used without further purification. 8-Hydroxy-6-nitroquinoline (**10**) was purchased from Apollo Scientific. Analytical thin-layer chromatography (TLC) was performed on Merck silica gel (60F₂₅₄) plates (0.25 mm). Preparative column chromatography was performed using Merck silica gel 60 (0.063–0.200 mm). ¹H NMR and ¹³C NMR spectra were recorded on a Bruker Avance 400 MHz NMR spectrometer at 295 K in CDCl₃ or DMSO-*d*₆ solutions. NMR spectra were processed and analyzed in MestReNova. Chemical shifts are given in parts per million (ppm) and are referenced to the deuterated solvent used. Coupling constants *J* are given in Hertz, and the splitting patterns are given as s (singlet), br s (broad singlet), d (doublet), dd, (doublet of doublets), t (triplet), q (quartet), or m (multiplet). Resonance assignments were made on the basis of one- and two-dimensional NMR techniques which include ¹H, ¹³C, COSY, HSQC, and HMBC experiments. High-resolution mass spectrometry (HRMS) was performed on a Thermo Scientific Q Exactive Plus mass spectrometer (Thermo Fisher Scientific, USA). The purity of the compounds was assessed *via* analytical reversed-phase UHPLC using a Thermo Scientific Dionex UltiMate 3000 UHPLC system (Thermo Fisher Scientific), equipped with a photodiode array detector at 254 nm. A Waters Acquity UPLC[®] HSS C18 SB column (1.8 μm, 2.1 mm × 50 mm) was used, thermostated at 40 °C. The mobile phase consisted of 0.1 % TFA in H₂O (A) and MeCN (B), employing the following gradient: 95 % A to 5 % A in 10 min, then 95 % B for 4 min, with flow rate of 0.3 mL min⁻¹ and injection volume of 5 μL. The purities of all test compounds used for the biological evaluations were ≥ 95 % by UHPLC analysis (detection at 254 nm).

Synthesis of 1,2,3,4-tetrahydroquinolin-8-ol (2). – To a solution of 8-hydroxyquinoline (726 mg, 5.0 mmol) in AcOH (20 mL), NaCNBH₃ (629 mg, 10.0 mmol) was added slowly at room

temperature. The reaction mixture was stirred at 60 °C for 24 h. The mixture was then poured into saturated aqueous solution of Na₂CO₃ (100 mL) and washed with CH₂Cl₂ (3 × 50 mL). The combined organic phases were dried with Na₂SO₄, filtered, and the solvent evaporated under reduced pressure. The compound was purified by column chromatography (CH₂Cl₂/MeOH, 30/1) to give an off-white solid (435 mg, 58 %). Spectral data were in accordance with previously published data (22); *R_f* = 0.56 (EtOAc/*n*-hexane 1/1).

Synthesis of 1-acetyl-1,2,3,4-tetrahydroquinolin-8-yl acetate (**3**). – To a cooled (0 °C) solution of compound **2** (815 mg, 5.46 mmol) in dry THF (8 mL), DIPEA (2.73 mL, 16.5 mmol) and CH₃COCl (0.78 mL, 11.0 mmol) were added. The reaction mixture was stirred at room temperature for 1 h. Then, H₂O (10 mL) and HCl (0.5 mol L⁻¹, 10 mL) were added and the mixture extracted with EtOAc (2 × 50 mL). The combined organic phases were dried with Na₂SO₄, filtered, and the solvent evaporated under reduced pressure to give an off-white solid (1.09 g, 86 %). Spectral data were in accordance with previously published data (23); *R_f* = 0.48 (EtOAc).

Synthesis of 1-(8-hydroxy-3,4-dihydroquinolin-1(2*H*)-yl)ethan-1-one (**4**). – Compound **3** (1.09 g, 4.67 mmol) was dissolved in THF (10 mL) and NaOH (1 mol L⁻¹, 5 mL) was added dropwise. After stirring the reaction mixture at room temperature for 1 h, HCl (2 mol L⁻¹, 20 mL) was added, followed by extraction with EtOAc (2 × 20 mL). The combined organic phases were dried with Na₂SO₄, filtered, and the solvent evaporated under reduced pressure. The compound was purified by column chromatography (CH₂Cl₂/MeOH, 30/1) to give a white solid (749 mg, 84 %). *R_f* = 0.48 (CH₂Cl₂/MeOH, 20/1).

Synthesis of 1-(8-hydroxy-6-nitro-3,4-dihydroquinolin-1(2H)-yl)ethan-1-one (5).— Compound **4** (100 mg, 0.52 mmol) was dissolved in AcOH (4 mL) and the solution cooled to 15 °C. A cooled (0 °C) HNO₃ (65 %, 48 µL, 0.73 mmol) was added drop-wise and the reaction mixture stirred at 15 °C for 10 min. Then, H₂SO₄ (97 %, 286 µL, 5.2 mmol) was added in two portions. The reaction mixture was stirred at 15 °C for 10 min and at room temperature for 30 min. The mixture was poured into saturated aqueous solution of K₂CO₃ (5 mL), followed by the addition of NaOH (2 mol L⁻¹) until pH of 9. The aqueous phase was extracted with EtOAc (2 × 10 mL), the combined organic phases dried with Na₂SO₄, filtered, and the solvent evaporated under reduced pressure. The compound was purified by column chromatography (CH₂Cl₂/MeOH, 60/1 to 30/1) to yield compound **5** as red solid (94 mg, 77 %). *R*_f = 0.52 (CH₂Cl₂/MeOH, 9/1).

Synthesis of 8-hydroxy-6-nitro-1,2,3,4-tetrahydroquinoline (6).— To a solution of compound **5** (12 mg, 0.05 mmol) in EtOH (2 mL), hydrazine hydrate (25 µL, 0.5 mmol) and NH₄I (7.4 mg, 0.05 mmol) were added. The mixture was stirred at 66 °C for 3 h and then CH₂Cl₂ (10 mL) was added. The organic layer was extracted with saturated aqueous solution of NaHCO₃ (10 mL), the organic phase dried with Na₂SO₄, filtered, and the solvent evaporated under reduced pressure. The compound was purified by column chromatography (CH₂Cl₂/MeOH, 30/1) to obtain **6** as a red solid (4.7 mg, 58 %). *R*_f = 0.39 (CH₂Cl₂/MeOH, 15/1).

Synthesis of 8-hydroxy-5-nitro-1,2,3,4-tetrahydroquinoline (7), 8-hydroxy-7-nitro-1,2,3,4-tetrahydroquinoline (8), and 8-hydroxy-5,7-dinitro-1,2,3,4-tetrahydroquinoline (9).— To a cooled (0 °C) solution of compound **2** (60 mg, 0.40 mmol) in H₂SO₄ (97 %, 3 mL), a nitrating mixture composed of HNO₃ (65 %, 1.1 equiv.) and H₂SO₄ (97 %, 2 mL) was added drop-wise at 0 °C. The mixture was poured into saturated aqueous solution of K₂CO₃ (5 mL), followed by the addition of NaOH (2 mol L⁻¹) until pH of 7. The aqueous phase was extracted with EtOAc

(2 × 10 mL), the combined organic phases dried with Na₂SO₄, filtered, and the solvent evaporated under reduced pressure. The compounds **7–9** were separated and purified by column chromatography using eluent systems defined below.

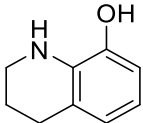
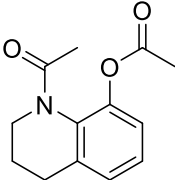
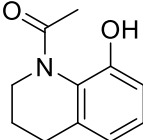
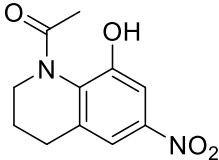
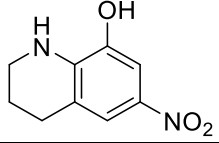
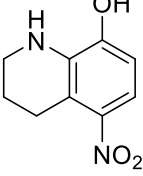
8-Hydroxy-5-nitro-1,2,3,4-tetrahydroquinoline (7). – Two consecutive column chromatographies using EtOAc/*n*-hexane, 1/2 and CH₂Cl₂/MeOH, 30/1 as eluents were used to obtain **7** as an orange solid (10 mg, 13 %). *R_f* = 0.49 (EtOAc/*n*-hexane, 1/1).

8-Hydroxy-7-nitro-1,2,3,4-tetrahydroquinoline (8). – Column chromatography using EtOAc/*n*-hexane, 1/2 was used to obtain **8** as an orange solid (3.9 mg, 5 %). *R_f* = 0.76 (EtOAc/*n*-hexane, 1/1).

8-Hydroxy-5,7-dinitro-1,2,3,4-tetrahydroquinoline (9). – Two consecutive column chromatographies using EtOAc/*n*-hexane, 1/2 and CH₂Cl₂/MeOH, 15/1 as eluents were used to obtain **9** an orange solid (4.8 mg, 5 %). *R_f* = 0.31 (EtOAc/*n*-hexane, 1/1).

Analytical and NMR spectral data of all compounds are given in Tables I and II.

Table I. Analytical data for compounds 2–10

Cpd	Structure	Chemical name	Molecular formula	HRMS	UHPLC purity
2		1,2,3,4-Tetrahydroquinolin-8-ol	C ₉ H ₁₁ NO	(ESI) m/z [M – H] [–] calcd. for C ₉ H ₁₀ NO, 148.0762; found, 148.0764	–
3		1-Acetyl-1,2,3,4-tetrahydroquinolin-8-yl acetate	C ₁₃ H ₁₅ NO ₃	(ESI) m/z [M + H] ⁺ calcd. for C ₁₃ H ₁₆ NO ₃ , 234.1125; found, 234.1123	–
4		1-(8-Hydroxy-3,4-dihydroquinolin-1(2H)-yl)ethan-1-one	C ₁₁ H ₁₃ NO ₂	(ESI) m/z [M + H] ⁺ calcd. for C ₁₁ H ₁₄ NO ₂ , 192.1019; found, 192.1017	–
5		1-(8-Hydroxy-6-nitro-3,4-dihydroquinolin-1(2H)-yl)ethan-1-one	C ₁₁ H ₁₂ N ₂ O ₄	(ESI) m/z [M – H] [–] calcd. for C ₁₁ H ₁₁ N ₂ O ₄ , 235.0724; found, 235.0724	–
6		8-Hydroxy-6-nitro-1,2,3,4-tetrahydroquinoline	C ₉ H ₁₀ N ₂ O ₃	(ESI) m/z [M + H] ⁺ calcd. for C ₉ H ₁₁ N ₂ O ₃ , 195.0770; found, 195.0774	95.79 % t_R = 8.81 min
7		8-Hydroxy-5-nitro-1,2,3,4-tetrahydroquinoline	C ₉ H ₁₀ N ₂ O ₃	(ESI) m/z [M – H] [–] calcd. for C ₉ H ₉ N ₂ O ₃ , 193.0613; found, 193.0616	97.45 % t_R = 5.01 min

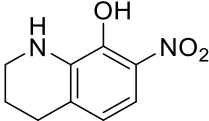
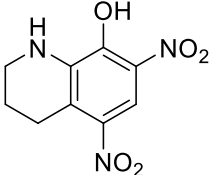
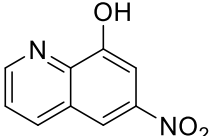
8		8-Hydroxy-7-nitro-1,2,3,4-tetrahydroquinoline	C ₉ H ₁₀ N ₂ O ₃	(ESI) <i>m/z</i> [M – H] [–] calcd. for C ₉ H ₉ N ₂ O ₃ , 193.0613; found, 193.0610	99.61 % <i>t</i> _R = 8.26 min
9		8-Hydroxy-5,7-dinitro-1,2,3,4-tetrahydroquinoline	C ₉ H ₉ N ₃ O ₅	(ESI) <i>m/z</i> [M – H] [–] calcd. for C ₉ H ₈ N ₃ O ₅ , 238.0464; found, 238.0469	98.78 % <i>t</i> _R = 11.20 min
10		8-Hydroxy-6-nitroquinoline	C ₉ H ₆ N ₂ O ₃	–	99.59 % <i>t</i> _R = 5.09 min

Table II. NMR spectral data for compounds 2–10

Cpd.	¹ H NMR (400 MHz)	¹³ C NMR (101 MHz)
2	¹ H NMR (400 MHz, DMSO- <i>d</i> ₆) δ 1.78 (sym m, 2H, H-3), 2.63 (t, <i>J</i> = 6.4 Hz, 2H, H-4), 3.19 (t, <i>J</i> = 5.5 Hz, 2H, H-2), 4.92 (br s, 1H, NH), 6.28 (t, <i>J</i> = 7.7 Hz, 1H, H-6), 6.28 – 6.38 (m, 1H, H-5), 6.45 (dd, <i>J</i> = 7.7, 1.5 Hz, 1H, H-7), 8.97 (s, 1H, OH)	¹³ C NMR (101 MHz, DMSO- <i>d</i> ₆) δ 21.77, 26.47, 40.89, 111.37, 114.68, 119.89, 120.31, 133.79, 143.18
3	¹ H NMR (400 MHz, CDCl ₃) δ 1.72 (br s, 1H, one H of H-3), 2.03 (s, 3H, NCOCH ₃), 2.19 (br s, 1H, one H of H-3), 2.25 (s, 3H, OCOCH ₃), 2.56 (br s, 1H, tetrahydroquinoline-H), 2.68 – 2.80 (m, 1H, tetrahydroquinoline-H), 2.88 (br s, 1H, tetrahydroquinoline-H), 4.56 (br s, 1H, tetrahydroquinoline-H), 6.99 (dd, <i>J</i> = 8.0, 1.4 Hz, 1H, H-5), 7.09 (app d, <i>J</i> = 7.3 Hz, 1H, H-7), 7.20 (t, <i>J</i> = 7.8 Hz, 1H, H-6)	¹³ C NMR (101 MHz, CDCl ₃) δ 20.74, 21.62, 24.02, 26.18, 41.08, 120.61, 125.57, 126.84, 132.90, 137.79, 144.47, 168.49, 170.65
4	¹ H NMR (400 MHz, CDCl ₃) δ 2.06 (p, <i>J</i> = 4.6 Hz, 2H, H-3), 2.37 (s, 3H, NCOCH ₃), 2.84 (app t, <i>J</i> = 7.5 Hz, 2H, H-4), 3.69 (t, <i>J</i> = 6.3 Hz,	¹³ C NMR (101 MHz, CDCl ₃) δ 23.22, 24.04, 26.33, 47.69, 118.17, 120.88, 127.25, 128.73, 133.08, 150.30, 171.51

	2H, H-2), 6.74 (dd, $J = 7.6, 1.3$ Hz, 1H, H-5), 6.91 (app d, $J = 8.2$ Hz, 1H, H-7), 7.10 (t, $J = 7.6$ Hz, 1H, H-6), 7.81 (s, 1H, OH)	
5	^1H NMR (400 MHz, DMSO- d_6) δ 1.78 – 1.94 (m, 2H, H-3), 1.98 (s, 3H, NCOCH ₃), 2.70 (t, $J = 6.3$ Hz, 2H, H-4), 3.44 – 3.80 (m, 2H, H-2), 7.60 (d, $J = 2.6$ Hz, 1H, H-7), 7.64 (dt, $J = 2.6, 0.9$ Hz, 1H, H-5), 10.82 (s, 1H, OH)	^{13}C NMR (101 MHz, DMSO- d_6) δ 20.67, 23.79, 26.01, 42.04, 105.98, 117.69, 118.08, 133.39, 142.17, 143.89, 170.03
6	^1H NMR (400 MHz, DMSO- d_6) δ 1.79 (p, $J = 6.1$ Hz, 2H, H-3), 2.73 (t, $J = 6.1$ Hz, 2H, H-4), 3.28 – 3.34 (m, 2H, H-2), 6.58 (br s, 1H, NH), 7.35 (d, $J = 2.5$ Hz, 1H, H-7), 7.46 (d, $J = 2.5$ Hz, 1H, H-5), 10.08 (s, 1H, OH)	^{13}C NMR (101 MHz, DMSO- d_6) δ 20.24 (C-3), 26.22 (C-4), 40.46 (C-2), 106.18 (C-7), 117.95, 118.03, 133.71, 141.59, 141.69
7	^1H NMR (400 MHz, DMSO- d_6) δ 1.76 (p, $J = 5.4$ Hz, 2H, H-3), 2.87 (t, $J = 6.4$ Hz, 2H, H-4), 3.21 (t, $J = 5.6$ Hz, 2H, H-2), 5.39 (br s, 1H, NH), 6.61 (d, $J = 8.7$ Hz, 1H, H-7), 7.15 (d, $J = 8.7$ Hz, 1H, H-6), 10.56 br (s, 1H, OH);	^{13}C NMR (101 MHz, DMSO- d_6) δ 20.81 (C-3), 24.45 (C-4), 40.16 (C-2), 109.99 (C-7), 112.82, 114.82, 134.87, 141.56, 148.11
8	^1H NMR (400 MHz, CDCl ₃) δ 1.96 (p, $J = 5.5$ Hz, 2H, H-3), 2.79 (t, $J = 6.4$ Hz, 2H, H-4), 3.39 (td, $J = 5.0, 2.1$ Hz, 2H, H-2), 4.50 (br s, 1H, NH), 6.58 (d, $J = 8.8$ Hz, 1H, H-5), 7.29 (d, $J = 8.8$ Hz, 1H, H-6), 10.81 br (s, 1H, OH)	—
9	^1H NMR (400 MHz, DMSO- d_6) δ 1.77 (p, $J = 5.5$ Hz, 2H, H-3), 2.90 (t, $J = 6.4$ Hz, 2H, H-4), 3.28 (t, $J = 5.5$ Hz, 2H, H-2), 7.79 (s, 1H, H-6), resonances for OH and NH missing; ^1H NMR (400 MHz, CDCl ₃) δ 1.96 (p, $J = 5.5$ Hz, 2H, H-3), 3.06 (t, $J = 6.4$ Hz, 2H, H-4), 3.46 (t, $J = 5.5$ Hz, 2H, H-2), 4.97 (br s, 1H, NH), 8.06 (s, 1H, H-6), 11.07 (br s, 1H, OH)	^{13}C NMR (101 MHz, DMSO- d_6) δ 19.58 (C-3), 24.37 (C-4), 39.85 (C-2), 127.55, 129.90, 131.62, 137.75, 140.58, 141.80
10	—	^{13}C NMR (101 MHz, DMSO- d_6) δ 104.34 (C-7), 114.39 (C-5), 123.57, 127.57, 138.51, 140.90, 145.57, 151.79, 154.86

Single crystal X-ray diffraction

X-ray diffraction data was collected on an Oxford Diffraction SuperNova diffractometer with Mo/Cu microfocus X-ray source with mirror optics and an Atlas detector at 150.00(10) K. Frames were processed and data reduced using CrysAlis PRO (Agilent Technologies Ltd, UK). The structures were solved in Olex2 (24) graphical user interface by direct methods implemented in SHELXT (25) and refined using olex2.refine (24). All non-hydrogen atoms were refined anisotropically. The hydrogen atoms were placed at calculated positions and treated using appropriate riding models. Figures were prepared using Mercury (26). The crystal structure has been submitted to the CCDC and allocated the deposition number 2428177. Additional details on structural properties and refinement details are given in the Supporting Information (Table S1 and Fig. S1).

Metal-chelating properties

The metal-chelating properties of nitroxoline analogs were evaluated in HEPES buffer (20 mmol L⁻¹, 150 mmol L⁻¹ NaCl, pH 7.4). Equimolar concentrations of CuCl₂, ZnCl₂, MgCl₂, CaCl₂, FeCl₂, and FeCl₃ were added to 30 μmol L⁻¹ solutions of the compounds (final concentration of DMSO was 1 %, V/V). The measurements were conducted on UV transparent 96-well microtiter plates (Corning® 96-well Clear Flat Bottom UV-Transparent Microplate, Catalogue Number 3635) using a microplate reader (Synergy HT, BioTek Instruments, Inc., USA). The FeCl₂ stock solution was prepared in the presence of 1 mmol L⁻¹ ascorbic acid to prevent oxidation of Fe²⁺. Formation of compound–metal ion complexes was detected through changes in the absorbance spectra following 1 hour of incubation.

MtMetAP1a and human MetAP2 inhibition

Nitroxoline analogs were first screened in 96-well plates at final concentrations of $125 \mu\text{mol L}^{-1}$ obtained by diluting 10 mmol L^{-1} DMSO stock solutions. Total reaction volume was $80 \mu\text{L}$. Each reaction contained 40 mmol L^{-1} HEPES (pH 7.5), 100 mmol L^{-1} NaCl, $100 \mu\text{mol L}^{-1}$ Met-AMC (L-methionine 7-amido-4-methylcoumarin) as a substrate, 200 nmol L^{-1} of respective ion (Co^{2+} , Mn^{2+} , Ni^{2+} or Fe^{2+}), 200 nmol L^{-1} MtMetAP1a and the tested compound. The final concentration of DMSO in the assay mixture was 1.25 % (V/V). In case of Fe^{2+} , sodium ascorbate was added to prevent oxidation (2:1 in respect to Fe^{2+} , *i.e.*, final concentration 400 nmol L^{-1}). Control reactions were carried out under the same conditions, but without the inhibitor and with 1.25 % (V/V) DMSO. All metal ions were used as chlorides. The assay was performed by first adding $1 \mu\text{L}$ of the compound stock solution into the well, followed by the addition of $10 \mu\text{L}$ of the enzyme, and finally, $69 \mu\text{L}$ of the substrate buffer solution containing the ion. The mixture was slightly shaken, and the measurement of fluorescence started immediately. For Fe^{2+} , the substrate buffer solution was left for 2 minutes after the addition of ascorbate to make a reducing environment and then used as usual. Residual activity (RA), expressed as the slope of the starting linear part of the detected signal, was recorded on Synergy H4 Hybrid Reader (BioTek Instruments, Inc.) using kinetic measurement (15 min, fluorescent detection, $\lambda_{\text{ex}} = 360 \text{ nm}$, $\lambda_{\text{em}} = 460 \text{ nm}$) and compared to the RA of the blank ($1 \mu\text{L}$ DMSO replacing the compound stock solution). Results were processed using Gen5 software (BioTek). Active compounds (residual activity below approx. 50 %) were used for the determination of IC_{50} . RA were plotted against $\log(c)$ using non-linear regression (four-parameter model) as implemented in GraphPad Prism 9.0.2 (GraphPad Software, USA). Measurements were done in triplicates with standard deviations within $\pm 10 \%$. As a positive control, we used clioquinol (CQ), a well-known inhibitor of MtMetAP1a (27).

The inhibition assays of human MetAP2 (R&D Systems, Inc., USA) were performed exactly as described by Shim *et al.* (14), whereby other cations beside Mn^{2+} were used.

Enzyme kinetics - enzyme and assay buffer

Human recombinant catB was expressed in *Escherichia coli* as reported previously (28). For the determination of catB endopeptidase and exopeptidase activities 100 mmol L⁻¹ phosphate buffer (pH 6.0) and 60 mmol L⁻¹ acetate buffer (pH 5.0) were used respectively. The assay buffers contained 0.1 % PEG 8000 (Sigma-Aldrich), 5 mmol L⁻¹ cysteine, and 1.5 mmol L⁻¹ EDTA. Prior to the assay, the enzymes were activated in the assay buffer for 5 min at 37 °C.

Determination of K_i values

CatB activity was measured using the specific fluorogenic substrates Z-Arg-Arg-AMC (Bachem, Switzerland) and Abz-Gly-Ile-Val-Arg-Ala-Lys(Dnp)-OH (Bachem) for CatB endopeptidase and exopeptidase activity, respectively. Inhibition constants were determined by measuring the reaction velocities at three substrate concentrations in the presence of seven concentrations of the inhibitor (0, 20, 40, 60, 80, 100, and 200 µmol L⁻¹). For the substrate Z-Arg-Arg-AMC, the concentrations of 60, 180, and 360 µmol L⁻¹ were used and for the substrate Abz-Gly-Ile-Val-Arg-Ala-Lys(Dnp)-OH, the concentrations of 1, 3, and 6 µmol L⁻¹ were used to assess catB endopeptidase and exopeptidase activity, respectively. The reaction was initiated by adding 90 µL of activated enzyme in the assay buffer at final concentrations of 5 nmol L⁻¹ and 0.5 nmol L⁻¹ for catB endopeptidase and exopeptidase activity, respectively, to the wells of a black microplate containing 5 µL of substrate and 5 µL of inhibitor. The formation of the fluorescent degradation products during the reaction was continuously monitored at emission 460 ± 10 nm with excitation at 380 ± 20 nm for substrate Z-Arg-Arg-AMC, and at emission 420 ± 10 nm, with excitation at 320 ± 20 nm for Abz-Gly-Ile-Val-Arg-Ala-Lys(Dnp)-OH at 37 °C on a Tecan Infinite M1000 (Switzerland) spectrofluorometer. All assay mixtures contained

5 % (V/V) DMSO. All measurements were performed in duplicate and repeated three times. The SigmaPlot® 12, Enzyme Kinetics Module™ 1.3 was used for calculation of K_i values.

Cell culture

MCF-10A neoT, a c-Ha-ras oncogene transfected human mammary epithelial cell line, was provided by Bonnie F. Sloane (Wayne State University, USA). MCF-10A neoT cells were provided by Bonnie F. Sloane (Wayne State University, USA). MCF-10A neoT cells were grown in Dulbecco's modified Eagle's medium (DMEM)/Nutrient Mixture F-12 (1:1) medium with GlutaMAX™ (Gibco, USA) supplemented with 5 % fetal bovine serum (FBS, Gibco), 1 $\mu\text{g mL}^{-1}$ insulin (Sigma-Aldrich), 0.5 $\mu\text{g mL}^{-1}$ hydrocortisone (Sigma-Aldrich), 20 ng mL^{-1} epithelial growth factor (Milipore, USA), and 1 % penicillin-streptomycin (Gibco), corresponding to 100 U mL^{-1} penicillin and 100 $\mu\text{g mL}^{-1}$ streptomycin. Cells were maintained at 37 °C in a humidified atmosphere of 5 % CO_2 until they reached 80 % confluency. Prior to their use, the cells were detached from the culture flasks with TripLE™ Select Enzyme (Gibco).

Cell viability assay

To determine the effect of nitroxoline derivatives on the cell viability of the MCF-10A neoT cells, an MTS (3-(4,5-dimethylthiazol-2-yl)-5-(3-carboxymethoxyphenyl)-2-(4-sulfophenyl)-2H-tetrazolium) colorimetric assay was used. Cells (3×10^4) were seeded into the wells of a 96-well microplate and incubated overnight to attach. The medium was replaced with 100 μL of medium containing the respective compound (at 1, 2.5, or 5 $\mu\text{mol L}^{-1}$) or DMSO (0.05 %). After incubation for 24 h, 10 μL of the reagent MTS was added to the wells, and following the incubation the absorbance of formazan was measured at 492 nm on a Tecan Infinite M1000 spectrofluorometer. The cell viability (%) was expressed as the ratio between absorbance in the presence of the compounds and in the presence of DMSO. All assays were performed in quadruplicate and repeated twice.

Intracellular DQ-collagen IV degradation assay

To determine the effect of nitroxoline derivatives on the degradation of EMC, its intracellular degradation was monitored using DQ-collagen IV. To monitor intracellular degradation of DQ-collagen type IV, flow cytometry was used. MCF-10A neoT cells were seeded at 6×10^4 cells/well into a 24-well plate and incubated overnight at 37 °C to attach. The cells were then treated with nitroxoline, its derivatives ($50 \mu\text{mol L}^{-1}$), or DMSO (0.5 %) in 500 μL serum-free medium (SFM) for 2 h at 37 °C. Then, DQ-collagen IV ($5 \mu\text{g mL}^{-1}$; Thermo Fischer, USA) was added, and the cells were incubated for an additional 2 h at 37 °C. The cells were detached and washed with phosphate-buffered saline (PBS). Propidium iodide ($10 \mu\text{g mL}^{-1}$; BD Bioscience) was added to exclude dead cells, and thus green fluorescence resulting from the degradation of DQ-collagen IV was monitored only for viable cells. The measurement was performed using the FACSCalibur system (BD Biosciences). The assay was performed in duplicates and repeated twice. FlowJo software was used for analysis of flow cytometry data.

Determination of antibacterial activities

Antimicrobial testing was carried out by the broth microdilution method in 96-well plate format following the CLSI guidelines and European Committee for Antimicrobial Susceptibility Testing recommendations. Bacterial suspension of specific bacterial strain equivalent to 0.5 McFarland turbidity standard was diluted with cation-adjusted Mueller Hinton broth to obtain a final inoculum of 10^5 CFU mL^{-1} . Compounds dissolved in DMSO and inoculum were mixed together and incubated for 20 h at 35 °C. After incubation, the minimal inhibitory concentration (MIC) values were determined by visual inspection as the lowest dilution of compounds showing no turbidity. The MICs were determined against *S. aureus* (ATCC 29213) and *E. coli* (ATCC 25922) bacterial strains. Tetracycline was used as a positive control on every assay

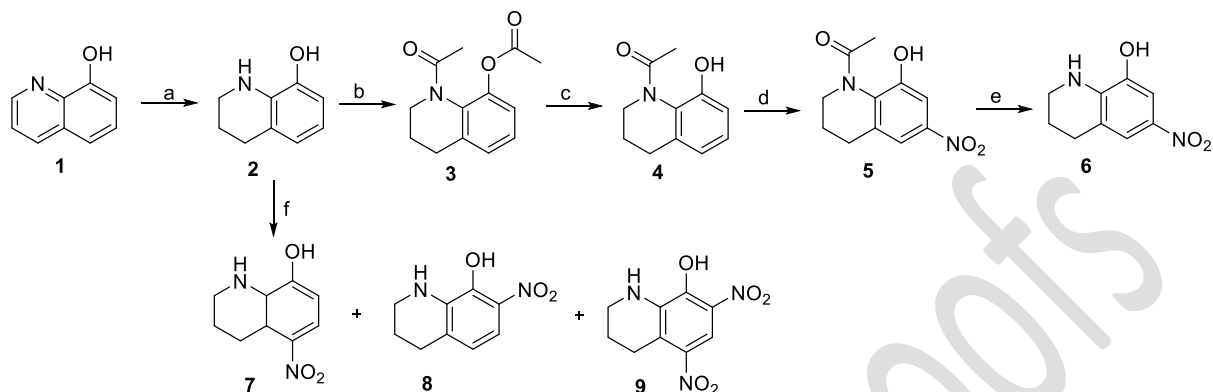
plate, showing *MIC* of 0.5 and 1 $\mu\text{g mL}^{-1}$ for *S. aureus* and *E. coli*, respectively. Antimicrobial testing for *M. smegmatis* was similar as described above, with small modifications. Bacterial suspension of bacterial strain equivalent to 0.5 McFarland turbidity standard was diluted with cation-adjusted Mueller Hinton broth w/OADC to obtain a final inoculum of $5 \times 10^5 \text{ CFU mL}^{-1}$. Compounds dissolved in DMSO and inoculum were mixed together and incubated for 6 days at 30 °C. After incubation the minimal inhibitory concentration (*MIC*) values were determined by visual inspection as the lowest dilution of compounds showing no turbidity. The *MICs* were determined against *M. smegmatis* bacterial strain. Isoniazid was used as a positive control showing *MIC* of 0.5–1 $\mu\text{g mL}^{-1}$.

RESULTS AND DISCUSSION

Synthesis

To prepare the partially saturated compounds, 8-hydroxyquinoline (**1**) was used as the starting reagent. In the first step, we applied $\text{Na}(\text{OAc})_3\text{BH}$ as a reducing agent to yield the 1,2,3,4-tetrahydroquinolin-8-ol (**2**), which was the main intermediate to prepare the 5-nitro and the 6-nitro partially saturated nitroquinoline counterparts **6–9**. 8-Hydroxy-6-nitro-1,2,3,4-tetrahydroquinoline (**6**) was obtained by initial diacetylation of compound **2** using acetyl chloride, followed by *O*-deprotection of 1-acetyl-1,2,3,4-tetrahydroquinolin-8-yl acetate (**3**) in alkaline conditions. Intermediate 1-(8-hydroxy-3,4-dihydroquinolin-1(2*H*)-yl)ethan-1-one (**4**) was then subjected to a nitration reaction using a 65 % HNO_3 /97 % H_2SO_4 mixture in AcOH to obtain 1-(8-hydroxy-6-nitro-3,4-dihydroquinolin-1(2*H*)-yl)ethan-1-one (**5**), which was subsequently deprotected by hydrazinolysis (29) (Scheme 1). 8-Hydroxy-5-nitro-1,2,3,4-tetrahydroquinoline (**7**), 8-hydroxy-7-nitro-1,2,3,4-tetrahydroquinoline (**8**), and 8-hydroxy-5,7-dinitro-1,2,3,4-tetrahydroquinoline (**9**) were prepared by a direct nitration of 1,2,3,4-

tetrahydroquinolin-8-ol (**2**) and several rounds of chromatographic separation to obtain sufficiently pure products (Scheme 1).



Scheme 1. Synthesis of 8-hydroxy-5-nitro- and 8-hydroxy-6-nitro-1,2,3,4-tetrahydroquinolines. Reagents and conditions: (a) $\text{Na}(\text{OAc})_3\text{BH}$, CH_3COOH , $60\text{ }^\circ\text{C}$, 24 h; (b) CH_3COCl , THF, rt, 1 h; (c) $1\text{ mol L}^{-1}\text{ NaOH}$, THF, rt, 1 h; (d) 65 % HNO_3 , 97 % H_2SO_4 , CH_3COOH , $16\text{ }^\circ\text{C}$ to rt, 1 h; (e) NH_2NH_2 , NH_4I , EtOH, $80\text{ }^\circ\text{C}$, 1 h; (f) 65 % HNO_3 /97 % H_2SO_4 , $0\text{ }^\circ\text{C}$ to $25\text{ }^\circ\text{C}$, 30 min.

It should be noted that we were quite surprised that the predominant product in the nitration of intermediate **4** was the 6-nitro analog (with nitro moiety positioned *meta* with respect to the 8-hydroxyl group). To confirm the formation of a 6-nitrated analog **6** (obtained after deprotection of **5**), two-dimensional NMR spectra were recorded, *i.e.* ^1H - ^1H homonuclear correlation spectroscopy (COSY) and nuclear Overhauser effect spectroscopy (NOESY). In the ^1H - ^1H COSY spectrum, couplings of H-3 (pentet at 1.79 ppm) with both H-4 (triplet at 2.73 ppm) and H-2 (symmetrical multiplet at 3.31 ppm) were clearly observed, together with coupling between H-2 and NH (singlet at 6.58 ppm), as well as between H-7 (doublet at 7.35 ppm) and H-5 (doublet at 7.46 ppm) (Fig. 2). Of note, the coupling constant between both aromatic protons was 2.5 ppm, which is characteristic for aromatic protons that are in the *meta* position. In

addition, a weak cross-peak between H-4 (triplet at 2.73 ppm) and H-5 (doublet at 7.46 ppm) was also seen (red dashed arrow in Fig. 2), thereby further suggesting that nitro group is at position 6 of the ring. The cross-peaks in the ^1H - ^1H NOESY spectrum (Fig. 3) indicated relevant through-space couplings between H-4 (triplet at 2.73 ppm) and H-5 (doublet at 7.46 ppm), H-2 (symmetrical multiplet at 3.31 ppm) and NH (singlet at 6.58 ppm), as well as between H-7 (doublet at 7.35 ppm) and OH (singlet at 10.08 ppm).

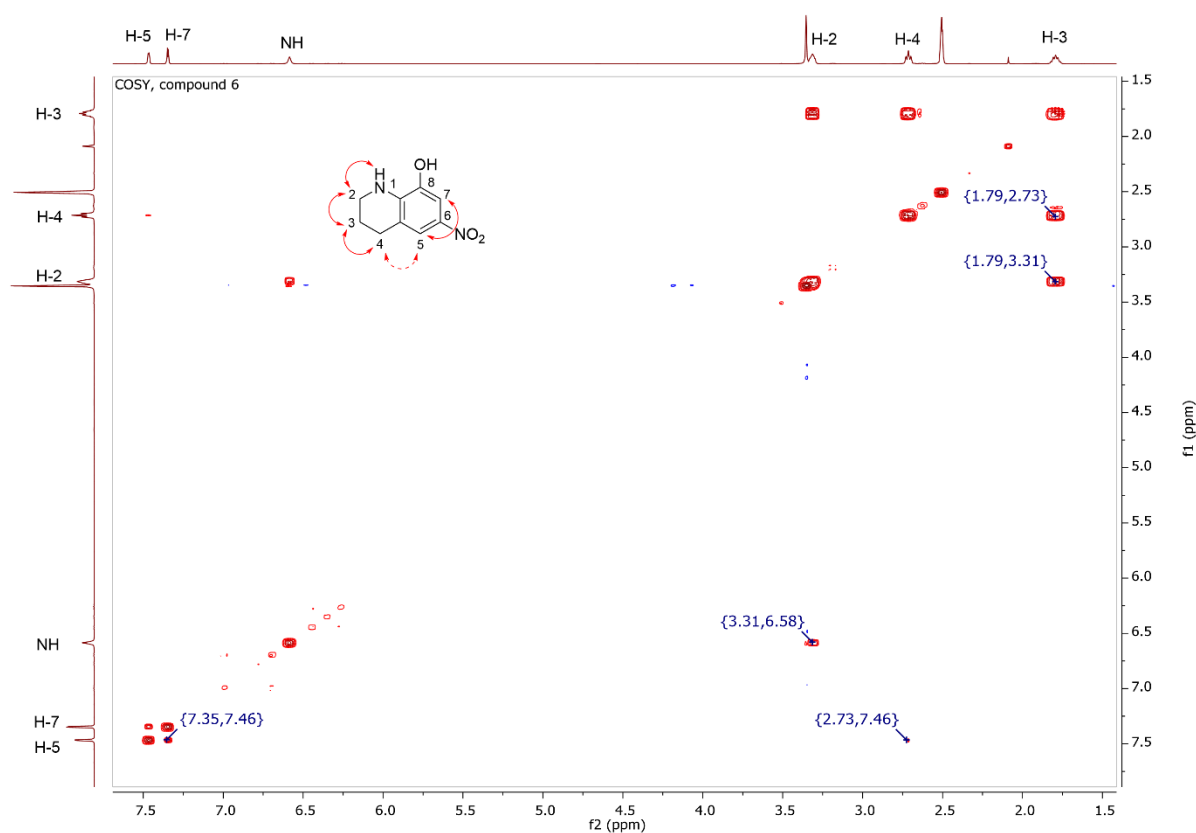


Fig. 2. Compound **6**, ^1H - ^1H COSY spectrum, $\text{DMSO}-d_6$. Cross-peaks that indicate coupling between protons H-3 and H-4, H-3 and H-2, H-2 and NH, H-7 and H-5 are noted.

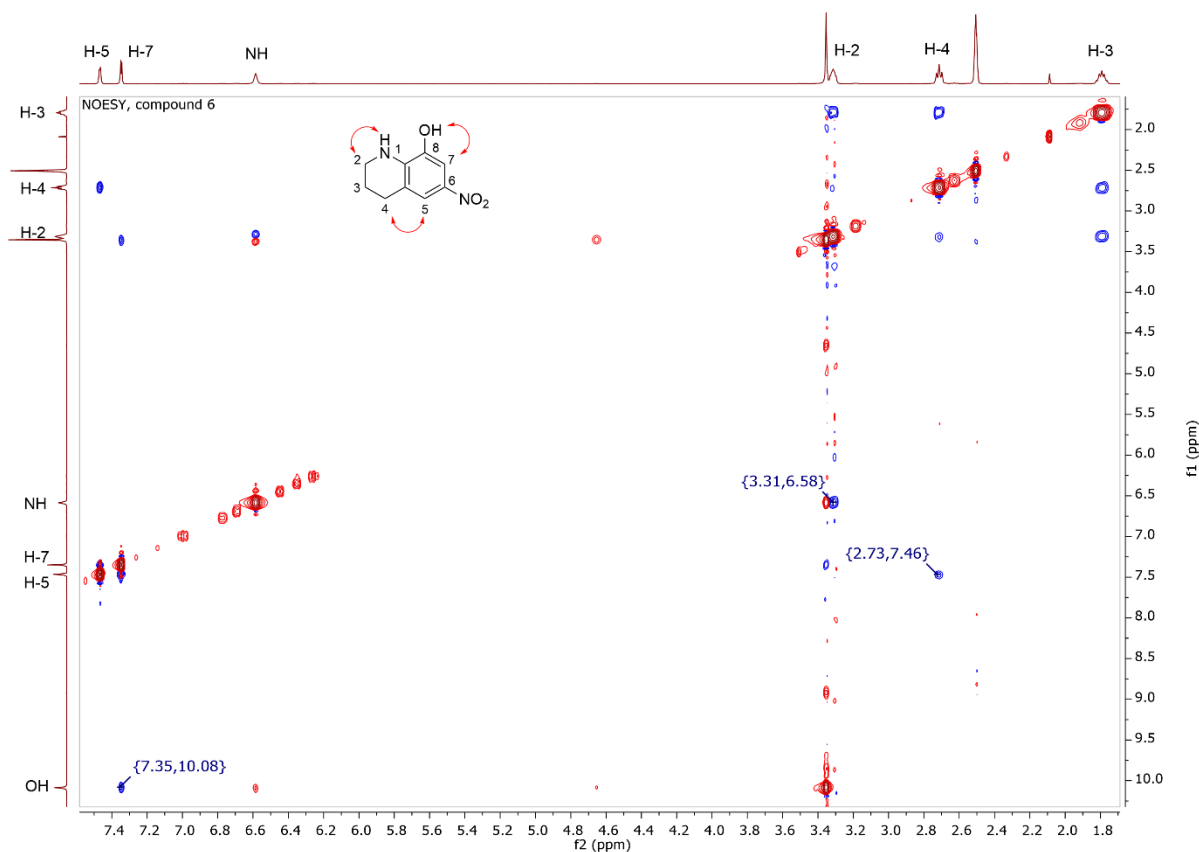


Fig. 3. Compound **6**, ^1H - ^1H NOESY spectrum, $\text{DMSO-}d_6$. Cross-peaks that indicate relevant through-space couplings are noted.

In addition, a crystal structure of compound **6** was solved (Fig. 4a), which unequivocally confirmed that nitro group in 1,2,3,4-tetrahydro nitroxoline analogs **5** and **6** is present at position 6. Compound **6** crystallizes in monoclinic space group $C2/c$. The structure shows the expected planarity of the *m*-nitrophenol ring with the fused piperidine ring in which the C3 atom is disordered between two positions above and below the aromatic plane (Fig. 4a). The crystal packing is influenced by three distinct directional hydrogen bonds forming a three-dimensional network (Fig. 4b). The hydroxyl group and the aromatic H7 atoms form a strong and a weak hydrogen bond with the nitro group oxygen atoms of the neighboring molecule ($d(\text{O8-H8}\cdots\text{O6B}') = 2.021 \text{ \AA}$, $d(\text{C7}_{(\text{Ar})}\text{-H7}\cdots\text{O6A}') = 2.362 \text{ \AA}$), while the amine H1 atom is

also involved in a weak hydrogen bond with the O6B atom of a third molecule of compound XY ($d(\text{N1-H1}\cdots\text{O6B''}) = 2.306 \text{ \AA}$).

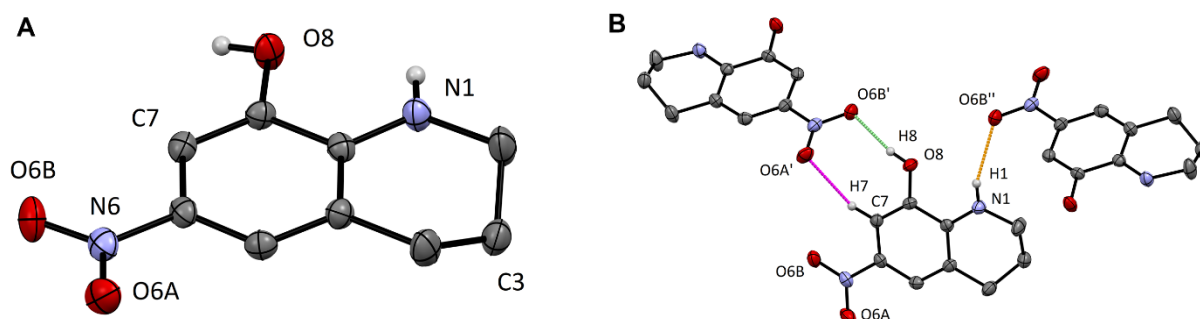


Fig. 4. a) Crystal structure of compound **6** with selected relevant atom labelling. Thermal ellipsoids are drawn at 50 % probability level and hydrogen atoms not bound to heteroatoms are omitted for better clarity; b) hydrogen bond network (lime O–H \cdots O, purple C–H \cdots O, and orange N–H \cdots O) in the crystal structure of compound **6**.

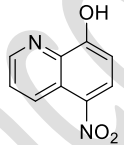
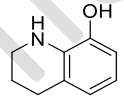
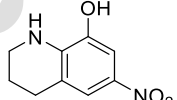
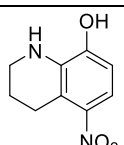
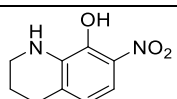
Biochemical evaluation

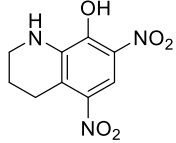
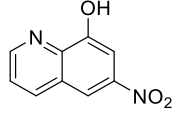
Metal-binding properties of nitroxoline analogs

The metal-binding properties of nitroxoline are central to many of its pharmacological effects, both as an antibacterial agent (4) and a potential anticancer drug (30). Its ability to chelate essential metal cations not only disrupts microbial growth but also shows promise in targeting cancer cells through increasing copper-dependent intracellular reactive oxygen species generation. Therefore, our first step in a cascade of assays was to explore the complexation capacity of compounds using UV-Vis spectroscopic measurements (31), whereby the changes of absorbance spectra in the presence and absence of equimolar amounts of selected metal chlorides (*i.e.*, CuCl₂, CaCl₂, MgCl₂, FeCl₃, ZnCl₂, and FeCl₂) were monitored. Because the 8-hydroxyquinoline fragment is essential for the chelating properties, it was not surprising that

1,2,3,4-tetrahydroquinoline analogs **2**, **6–9** did not form complexes with the metal ions used as the nitrogen electron pairs are delocalized in the aromatic systems of the molecules (Table III). On the other hand, interactions of Cu^{2+} , Zn^{2+} and Fe^{2+} with 8-hydroxy-6-nitroquinoline (**10**, Table III) induced a hypsochormic and hypochromic shift of its absorbance maximum at around 275 nm with clear isosbestic points present approximately 300 nm confirming the complexation. Similarly, a hypsochromic and hyperchromic change was observed in the presence of Fe^{3+} ions, indicating the formation of metal-ligand complexes (Fig. 5). Note that no change in the absorbance spectra of compound **10** was detected in the presence of Ca^{2+} and Mg^{2+} ions, which is very similar to what we previously determined for nitroxoline (Table III) (31).

Table III. Qualitative assessment of interactions of nitroxoline derivatives with selected metal ions in 1:1 (mol. eq.) mixtures in aqueous solutions at $30 \mu\text{mol L}^{-1}$ concentrations

Cpd.	Structure	Chelation					
		Cu^{2+}	Ca^{2+}	Mg^{2+}	Fe^{3+}	Zn^{2+}	Fe^{2+}
nitroxoline ^a		yes	no	no	no	yes	yes
2		no	no	no	no	no	no
6		no	no	no	no	no	no
7		no	no	no	no	no	no
8		no	no	no	no	no	no

9		no	no	no	no	no	no
10		yes	no	no	yes	yes	yes

^a Data from Ref 31.

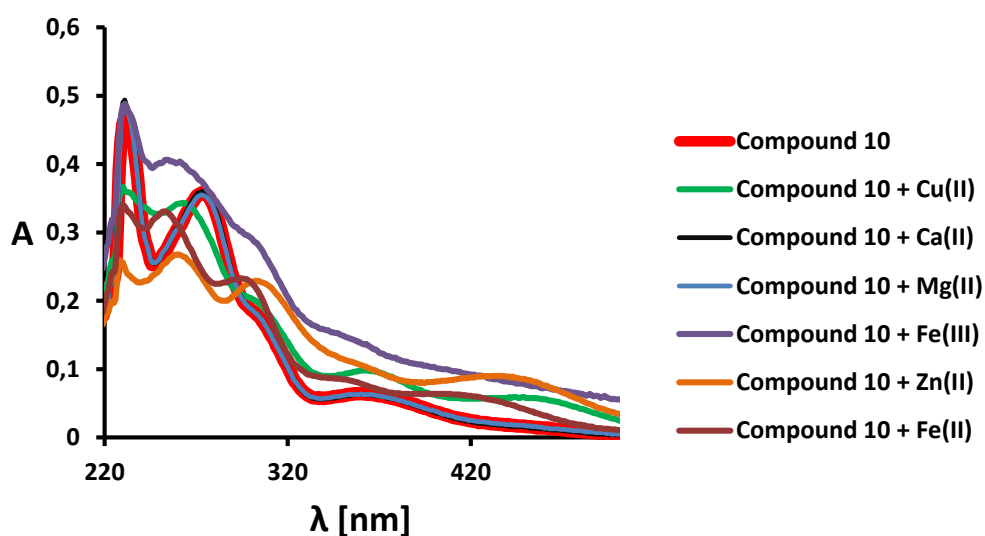


Fig. 5. Metal-chelation properties of compound **10**. Absorption spectra changes for compound **10** (30 $\mu\text{mol L}^{-1}$ concentration) incubated with different metal ions at equimolar concentrations.

Inhibition of MetAP1a from Mycobacterium tuberculosis and human MetAP2

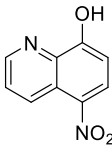
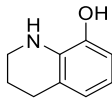
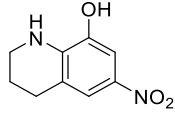
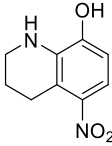
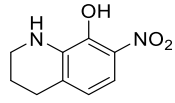
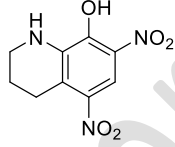
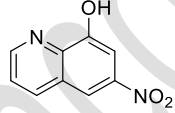
MetAPs are essential and ubiquitously expressed metalloproteases that remove the N-terminal methionine from proteins and peptides (32). Because of their importance as a pharmacological target (33) and because nitroxoline and other 8-hydroxyquinoline derivatives were shown to inhibit MetAPs from different species (14, 27, 34), our next step was to evaluate the prepared compounds against MetAP1a from *M. tuberculosis* (MtMetAP1a) and against human MetAP2. We performed inhibition assays in the presence of four different divalent cations, *i.e.*, Co^{2+} , Mn^{2+} , Ni^{2+} , and Fe^{2+} . Namely, it is known that the type of metal cation in the active site of

MetAPs affects both the activity of the enzyme and the inhibitory activities of the evaluated compounds (35, 36).

The assays on human MetAP2 showed that conversion of the core quinoline ring to the partially saturated 1,2,3,4-tetrahydroquinoline counterparts generally led to slightly diminished inhibition (see for example nitroxoline and compound **7**, Table IV). The 6-nitro regioisomer **10** performed worse in comparison to nitroxoline only when Mn^{2+} and Fe^{2+} were used as cations, whereas in the presence of Co^{2+} and Ni^{2+} inhibition of MetAP2 remained approximately the same. As expected, compound **6** with two structural modifications inhibited MetAP2 to a bit lower extent than nitroxoline (Table IV), but this inhibition was very balanced and independent of the metal cofactor. Assays with a mycobacterial homolog showed that partial saturation of the quinoline ring led to abrogation of MtMetAP1a inhibition when Mn^{2+} , Ni^{2+} , and Fe^{2+} were used as cofactors. Interestingly, in the presence of Co^{2+} these derivatives proved to be better inhibitors in comparison to nitroxoline, with compound **6** being the most potent with IC_{50} value of $89 \mu\text{mol L}^{-1}$ (Table IV). It should also be noted that compound **10** inhibited MetAP1a in low micromolar range and more potently than nitroxoline regardless of the metal cofactor used in the assay (Table IV).

In summary, partially saturated derivatives showed diminished inhibition of MetAPs, which is most probably due to their inability to chelate divalent ions (34, 37). However, the fact that 8-hydroxy-6-nitro-1,2,3,4-tetrahydroquinoline (**6**) inhibited MetAP2 regardless of the cofactor makes it a solid starting point for further optimization towards more potent MetAP inhibitors, which would not rely on chelation of the metal ion within the enzyme's active site. Compound **10**, on the other hand, can also be deemed as a promising hit for further development, because it inhibited both MetAPs in the low micromolar range. Its mechanism of action is, however, most probably related to interference with the metal cofactor.

Table IV. Inhibitory activities of the prepared nitroxoline analogs against MtMetAP1a and human MetAP2

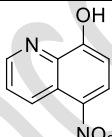
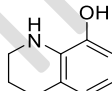
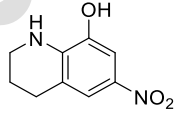
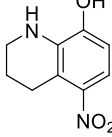
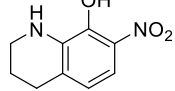
Cpd.	Structure	MtMetAP1a IC_{50} ($\mu\text{mol L}^{-1}$) ^a				MetAP2 IC_{50} ($\mu\text{mol L}^{-1}$) ^a			
		Co ²⁺	Mn ²⁺	Ni ²⁺	Fe ²⁺	Co ²⁺	Mn ²⁺	Ni ²⁺	Fe ²⁺
nitroxoline		339	34	n.i.	44	5	0.23	39	2
2		226	74	n.i.	n.i.	6	5	n.i.	17
6		89	86	n.i.	n.i.	36	45	38	16
7		288	n.i.	n.i.	n.i.	18	2	n.i.	9
8		91	n.i.	n.i.	n.i.	68	24	n.i.	24
9		n.i.	n.i.	n.i.	n.i.	29	7	n.i.	n.i.
10		91	34	40	9	4	19	21	258

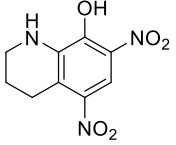
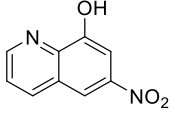
^a IC_{50} values are the mean \pm SD ($n = 3$). SDs are not included (for clarity) and were within ± 10 %. n.i. Residual activity (RA) > 50 % at $125 \mu\text{mol L}^{-1}$ of compound. Clioquinol, a positive control, inhibited MtMetAP1 in the presence of Co²⁺ and Fe²⁺ with IC_{50} values of 11 and 101 $\mu\text{mol L}^{-1}$, respectively, whereas the RA values in the presence of Mn²⁺ and Ni²⁺ were 57 and 50 %, respectively.

Antibacterial activities

All compounds were next tested for *in vitro* antibacterial activity against *M. smegmatis*, *E. coli*, and *S. aureus* (Table V). Most derivatives were unfortunately found to be weaker inhibitors of bacterial growth in comparison to nitroxoline. For example, the 8-hydroxy-7-nitro-1,2,3,4-tetrahydroquinoline **1** (**8**) showed no antibacterial activity, whereas the 8-hydroxy-5,7-dinitro-1,2,3,4-tetrahydroquinoline (**9**) and 8-hydroxy-5-nitro-1,2,3,4-tetrahydroquinoline (**7**) showed antibacterial characteristics only against *S. aureus* ($MIC = 16 \mu\text{g mL}^{-1}$) and *M. smegmatis* ($MIC = 32 \mu\text{mol L}^{-1}$), respectively (Table V). The most promising results were obtained for the 8-hydroxy-6-nitroquinoline (**10**); although this compound showed an 8-fold worse minimum inhibitory concentration (MIC) value for *M. smegmatis* and *E. coli* than nitroxoline, it did show a 4–8-fold improvement of MIC value for *S. aureus* ($MIC = 1\text{--}2 \mu\text{g mL}^{-1}$; Table V). It can be, therefore, summarized that nitroxoline exhibits more effective antibacterial activity than its analogs, which confirms that the introduction of saturation into the structure of nitroxoline or migration of the nitro group do not contribute to the improvement of antibacterial activity.

Table V. Antibacterial activities of nitroxoline and its derivatives

Cpd.	Structure	MIC (<i>M. smegmatis</i>) ($\mu\text{mol L}^{-1}$)	MIC (<i>E. coli</i>) ($\mu\text{g mL}^{-1}$)	MIC (<i>S. aureus</i>) ($\mu\text{g mL}^{-1}$)
nitroxoline		32	4	8
2		> 250	> 128	64
6		250	> 128	> 128
7		32	> 128	128
8		> 250	> 128	> 128

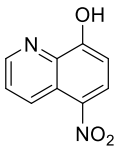
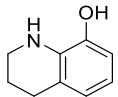
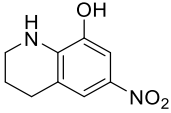
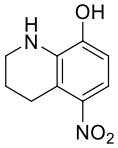
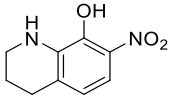
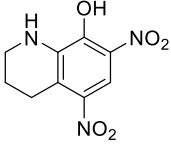
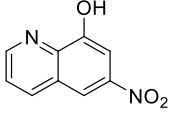
9		> 250	> 128	16
10		125	32	1-2

Inhibition of cathepsin B

Nitroxoline's ability to inhibit catB, an enzyme involved in tumor progression and metastasis, prompted us to evaluate the prepared derivatives for their inhibition of catB endopeptidase and exopeptidase activities, using specific substrates Z-Arg-Arg-7-amido-4-methylcoumarin (Z-Arg-Arg-AMC) and 2-aminobenzoyl (Abz)-Gly-Ile-Val-Arg-Ala-Lys(Dnp)-OH, whereby their kinetic parameters and mode of inhibition were determined. At this point it should be noted that nitroxoline does not share the prototypical structure of peptidomimetic, substrate-analogous inhibitors of catB (38). Interestingly, a 5- to 6-nitroquinoline group shift (compound **10**) led to significant decrease in inhibition of both catB activities in comparison to nitroxoline (Table VI). In addition, the partial saturation of the quinoline scaffold (compound **7**) also abolished inhibition of catB. On the other hand, compound **6** with two modifications incorporated into a single structure showed comparable inhibitory activities to nitroxoline. 8-Hydroxy-6-nitro-1,2,3,4-tetrahydroquinoline (**6**) acted as an uncompetitive inhibitor ($K_i' = 67 \pm 12 \mu\text{mol L}^{-1}$) of catB endopeptidase activity and as a noncompetitive inhibitor ($K_i = 185 \pm 27 \mu\text{mol L}^{-1}$) of the enzyme's exopeptidase activity (Table VI). Similar inhibitory characteristics were determined also for the 5,7-dinitro analog **9** (Table VI); however, this compound was determined to be an uncompetitive inhibitor of catB exopeptidase activity, with a K_i' value of $143 \pm 13 \mu\text{mol L}^{-1}$.

Table VI. Cathepsin B inhibitory activities of the prepared nitroxoline analogs

Cpd.	Structure	Z-Arg-Arg-AMC	Abz-Gly-Ile-Val-Arg-Ala-Lys(Dnp)-OH
------	-----------	---------------	-------------------------------------

		K_i ($\mu\text{mol L}^{-1}$) ^a	K_i' ($\mu\text{mol L}^{-1}$) ^a	K_i ($\mu\text{mol L}^{-1}$) ^a	K_i' ($\mu\text{mol L}^{-1}$) ^a
nitroxoline ^b		154 ± 27^c	40 ± 3^c	272 ± 11^d	
2		-	494 ± 40^e	n.i.	
6		-	67 ± 12^e	185 ± 27^d	
7		763 ± 1^d		-	317 ± 49^e
8		n.i.		295 ± 6^d	
9		-	91 ± 8^e	-	143 ± 13^e
10		-	366 ± 61^e	-	320 ± 72^e

^a K_i and K_i' values are the mean \pm SD ($n = 3$); ^b inhibition data published previously (13); ^c mixed inhibition; ^d noncompetitive inhibition; ^e uncompetitive inhibition; n.i. – no inhibition.

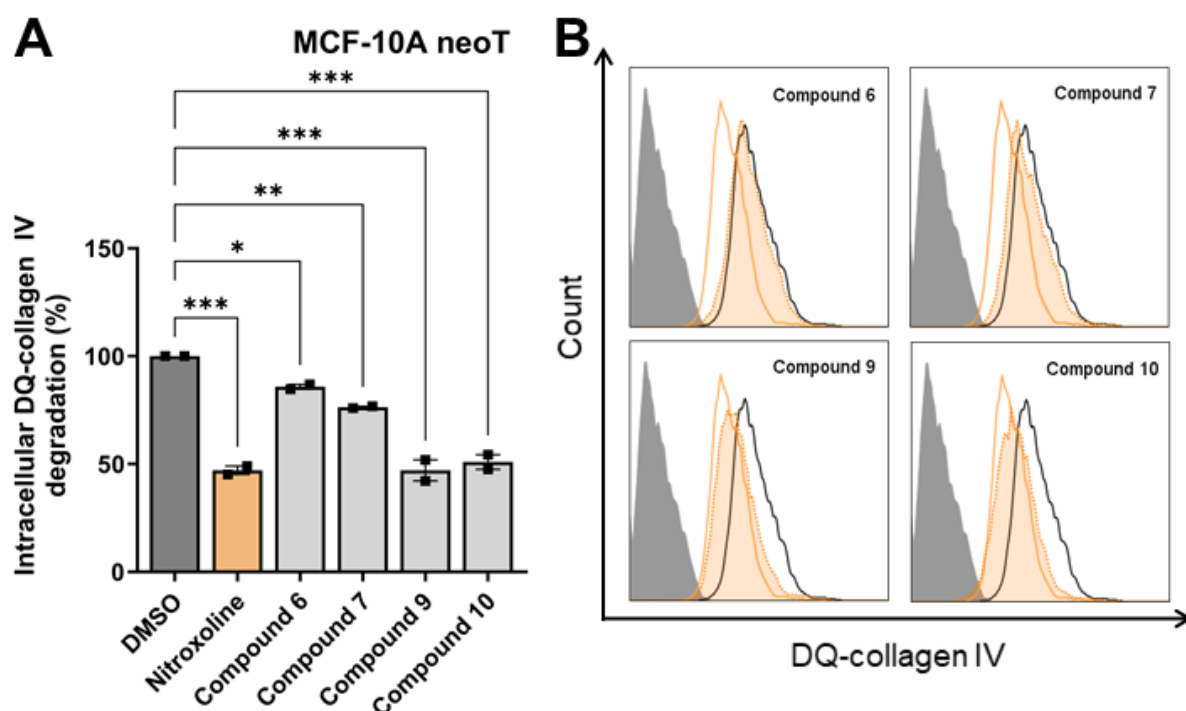


Fig. 6. Nitroxoline derivatives impair intracellular degradation of ECM by MCF-10A neoT cells. a) Reduction of intracellular DQ-collagen IV by MCF-10A neoT cells (6×10^4) in the presence of DMSO or suitable compound ($50 \mu\text{mol L}^{-1}$) as assayed by flow cytometry. Data are presented as means \pm SEM ($n = 2$) and experiments were performed in duplicates. * $p < 0.05$, ** $p < 0.01$, *** $p < 0.001$ (one-way ANOVA); b) intracellular DQ-collagen IV degradation after treatment with DMSO (solid black line), nitroxoline ($50 \mu\text{mol L}^{-1}$, solid orange line) or respective compound ($50 \mu\text{mol L}^{-1}$; dotted orange line, tinted) shown as change in the fluorescence intensity as measured by flow cytometer. Gray histograms denote unlabeled cells.

Impairment of degradation of the extracellular matrix

Since nitroxoline and its derivatives were previously shown to significantly inhibit extracellular and intracellular degradation of the extracellular matrix (ECM) (13, 39, 40), we next assessed the ability of selected compounds to inhibit intracellular collagen type IV degradation by MCF-

10A neoT cells (41). To achieve this, the fluorescein-labeled derivative of collagen IV (*i.e.*, DQ-collagen type IV) that gives bright green fluorescence upon proteolysis was used. As seen in Fig. 6, compounds **6**, **7**, **9**, and **10** all inhibited intracellular DQ-collagen IV degradation with the 8-hydroxy-5,7-dinitro-1,2,3,4-tetrahydroquinoline (**9**) and the 8-hydroxy-6-nitroquinoline (**10**) exhibiting similarly potent effect as nitroxoline. Interestingly, despite that analog **6** was the most potent catB inhibitor (Table VI) it showed only ~20 % reduction of intracellular DQ-collagen IV degradation. The partially saturated nitroxoline analog **7** also showed reduced effect in this cell-based assay in comparison to the parent nitroxoline (Fig. 3). Of note, all compounds were shown to be nontoxic on MCF-10A neoT cells up to a concentration of 5 μ M as determined by an MTS assay (Fig. 7).

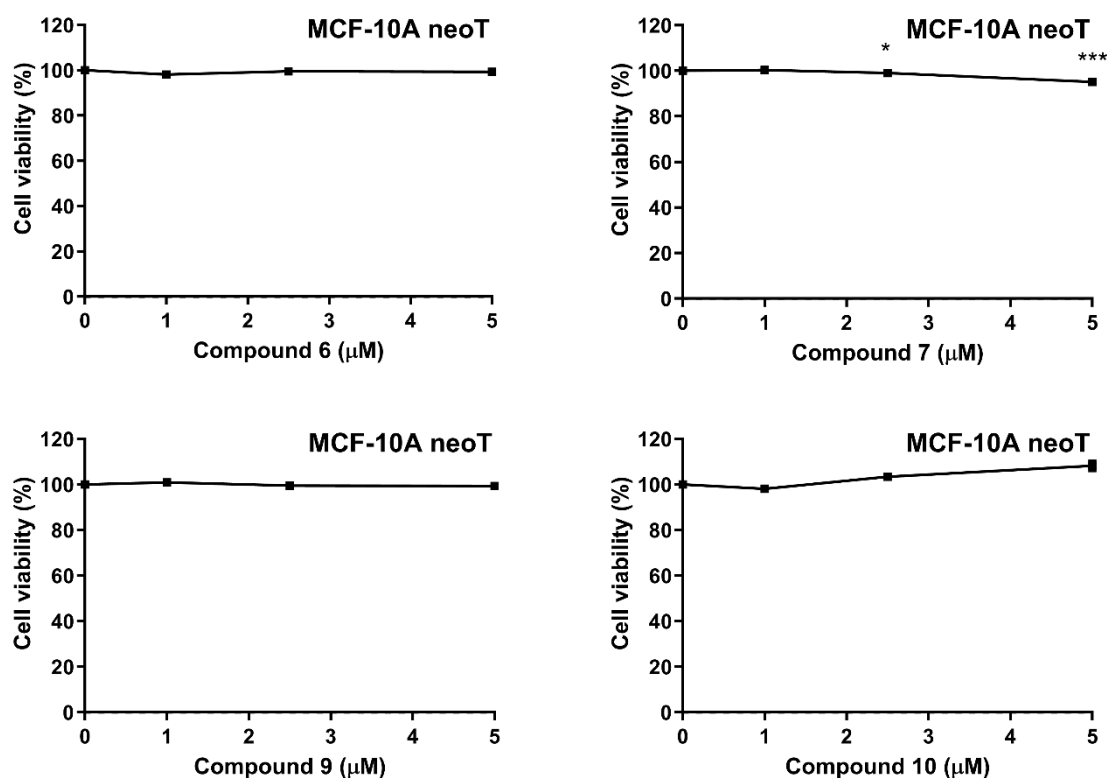


Fig. 7. Cytotoxicity of nitroxoline derivatives on MCF-10A neoT cells as determined by MTS assay. MCF-10A neoT cells were treated with increasing concentrations of compounds for 24

h and afterwards MTS reagent was added. Data are presented as percentage of viable cells from two independent experiments (mean \pm SEM) in the presence of the inhibitor compared to DMSO, used as a control. The experiments were performed in quadruplicate. * $p < 0.05$, ** $p < 0.01$, *** $p < 0.001$.

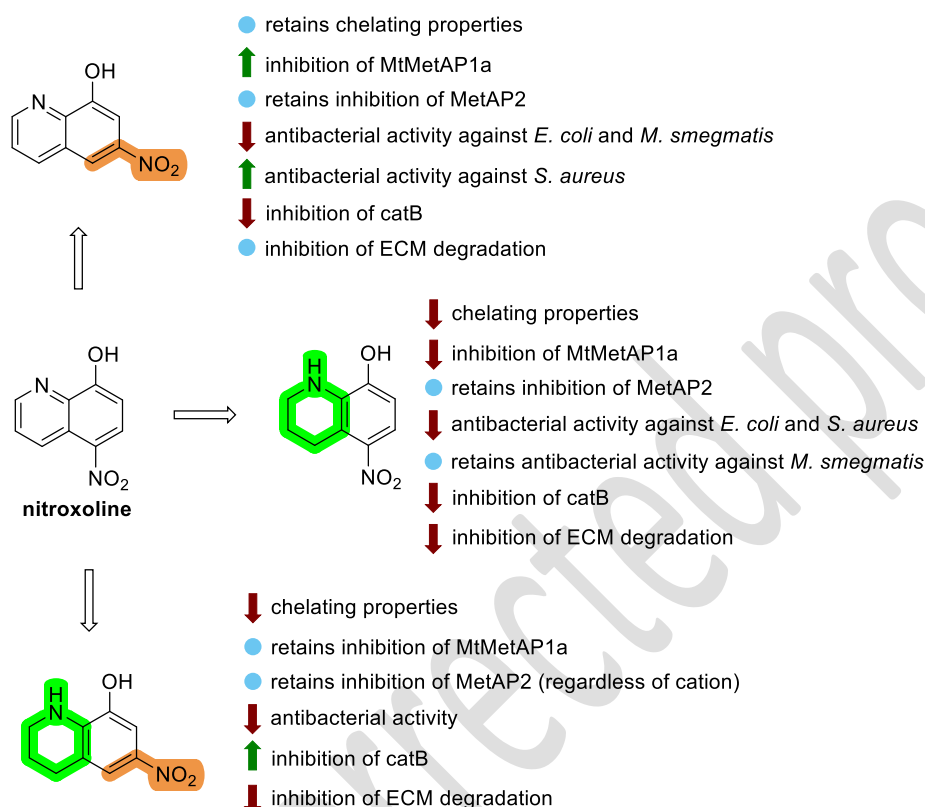


Fig. 8. A summary of characteristics of nitroxoline analogs that show trends in changes of biological activities.

CONCLUSIONS

Nitroxoline and its analogs received a lot of attention due to the variety of their pharmacological activities, ranging from antibacterial to antitumor. Here, we prepared a small series of nitroxoline analogs that were either partially saturated, had nitro group at position 6, or had both of these changes incorporated in a single molecule. These compounds were then subjected to a variety of assays and the results for most interesting compounds are summarized in Fig. 8.

When testing metal chelating properties of compounds using UV-Vis spectrometry measurements, we demonstrated that partial saturation of the quinoline ring leads to loss of chelating properties. The 8-hydroxy-6-nitroquinoline (**10**), on the other hand, retained chelating abilities. The inability to chelate divalent ions was most probably the reason that 1,2,3,4-tetrahydro analogs showed diminished inhibition of MetAPs. However, the fact that compound **6** was able to inhibit human MetAP2 independently of the metal cofactor makes it an interesting hit for further development. Partial quinoline ring saturation was the most detrimental to antibacterial potency of derivatives, which is undoubtedly related to loss of the ability of ion chelation. Only the 6-nitro analog **10** showed some antibacterial activity and even this was lower than determined for nitroxoline in two out of three strains. To demonstrate the potential of compound **10** for further development, assays on a significantly expanded set of bacterial strains would be needed. Most changes also abolished catB inhibition, as only 8-hydroxy-6-nitro-1,2,3,4-tetrahydroquinoline (**6**) the 5,7-dinitro analog **9** retained similarly potent inhibition as nitroxoline. The latter was also the most potent in inhibiting the intracellular DQ-collagen IV degradation. In conclusion, this work represents an expansion of the chemical space of nitroxoline analogs and despite suboptimal results in terms of pharmacological activities, compounds **6** and **10** are solid starting points for future hit optimization campaigns.

Acknowledgments. – The authors acknowledge the financial support from the Slovenian Research and Innovation Agency – ARIS (core financing P1-0208, P4-0127, and P1-0175). Our sincere thanks go to Dr. Kaja Berg who was vital for the initial assays with MtMetAP1a, performed in the research group of prof. Courtney Aldrich at the College of Pharmacy, University of Minnesota. The authors also acknowledge the support of the Centre for Research Infrastructure at the University of Ljubljana, Faculty of Chemistry and Chemical Technology, which is part of the Network of Research and Infrastructural Centres UL (MRIC UL) and is

financially supported by the ARIS (Infrastructure programme No. IO-0022) for the use of the Supernova diffractometer.

Conflict of interest. – The authors declare no competing financial interest in connection with this manuscript.

Authors contributions. – Conceptualization, D.K., J.K., S.G., and I.S.; methodology, D.K., M.H., A.M., and J.K.L.; analysis, D.K. and I.S.; biochemical measurements, D.K., M.H., and A.M.; funding acquisition, I.S. and S.G.; writing, original draft preparation, I.S.; writing, review and editing, all authors. All authors have read and agreed to the published version of the manuscript.

REFERENCES

1. K. G. Naber, H. Niggemann, G. Stein and G. Stein, Review of the literature and individual patients' data meta-analysis on efficacy and tolerance of nitroxoline in the treatment of uncomplicated urinary tract infections, *BMC Infect. Dis.* **14** (2014) Article ID 628 (16 pages); <https://doi.org/10.1186/s12879-014-0628-7>
2. C. Pelletier, P. Prognon and P. Bourlioux, Roles of divalent cations and pH in mechanism of action of nitroxoline against *Escherichia coli* strains, *Antimicrob. Agents Chemother.* **39**(3) (1995) 707–713; <https://doi.org/10.1128/aac.39.3.707>
3. B. Murugasu-Oei and T. Dick, In vitro activity of the chelating agents nitroxoline and oxine against *Mycobacterium bovis* BCG, *Int. J. Antimicrob. Agents* **18**(6) (2001) 579–582; [https://doi.org/10.1016/S0924-8579\(01\)00437-X](https://doi.org/10.1016/S0924-8579(01)00437-X)
4. E. Cacace, M. Tietgen, M. Steinhauer, A. Mateus, T. G. Schultze, M. Eckermann, M. Galardini, V. Varik, A. Koumoutsi, J. J. Parzeller, F. Corona, A. Orakov, M. Knopp, A.

- Brauer-Nikonow, P. Bork, C. V. Romao, M. Zimmermann, P. Cloetens, M. M. Savitski, A. Typas and S. Göttig, Uncovering nitroxoline activity spectrum, mode of action and resistance across Gram-negative bacteria, *Nat. Commun.* **(16)** (2025) Article ID 3783 (16 pages); <https://doi.org/10.1038/s41467-025-58730-5>
5. A. Sobke, M. Klinger, B. Hermann, S. Sachse, S. Nietzsche, O. Makarewicz, P. M. Keller, W. Pfister and E. Straube, The urinary antibiotic 5-nitro-8-hydroxyquinoline (nitroxoline) reduces the formation and induces the dispersal of *Pseudomonas aeruginosa* biofilms by chelation of iron and zinc, *Antimicrob. Agents Chemother.* **56**(11) (2012) 6021–6025; <https://doi.org/10.1128/AAC.01484-12>
 6. M. R. Jacobs, R. G. Robinson and H. J. Koornhof, Antibacterial activity of nitroxoline and sulphamethizole alone and in combination in urinary tract infections, *S. Afr. Med. J.* **54**(23) (1978) 959–962; https://journals.co.za/doi/abs/10.10520/AJA20785135_19317
 7. R. Wykowski, A. M. Fuentefria and S. F. Andrade, Antimicrobial activity of clioquinol and nitroxoline: a scoping review, *Arch. Microbiol.* **204** (2022) Article ID 535 (31 pages); <https://doi.org/10.1007/s00203-022-03122-2>
 8. F. Fuchs, F. Becerra-Aparicio, K. Xanthopoulou K, H. Seifert and P. G. Higgins, *In vitro* activity of nitroxoline against carbapenem-resistant *Acinetobacter baumannii* isolated from the urinary tract, *J. Antimicrob. Chemother.* **77**(7) (2022) 1912–1915; <https://doi.org/10.1093/jac/dkac123>
 9. H. Hof and C. Juretschke, Nitroxoline: an option for the treatment of urinary tract infection with multi-resistant uropathogenic bacteria, *Infection* **47** (2019) 493–495; <https://doi.org/10.1007/s15010-018-1253-y>
 10. A. M. Hoffmann, M. Wolke, J. Rybniker, G. Plum and F. Fuchs, *In vitro* activity of repurposed nitroxoline against clinically isolated mycobacteria including multidrug-

- resistant *Mycobacterium tuberculosis*, *Front. Pharmacol.* **13** (2022) Article ID 906097 (6 pages); <https://doi.org/10.3389/fphar.2022.906097>
11. Y. Abouelhassan, Q. Yang, H. Yousaf, M. T. Nguyen, M. Rolfe, G. S. Schultz and R. W. Huigens, Nitroxoline: a broad-spectrum biofilm-eradicating agent against pathogenic bacteria. *Int. J. Antimicrob. Agents* **49**(2) (2017) 247–251; <https://doi.org/10.1016/j.ijantimicag.2016.10.017>
 12. A. Proschak, G. Martinelli, D. Frank D, M. J. Rotter, S. Brunst, L. Weizel, L. D. Burgers, R. Fürst, E. Proschak, I. Sosič, S. Gobec and T. A. Wichelhaus, Nitroxoline and its derivatives are potent inhibitors of metallo-beta-lactamases, *Eur. J. Med. Chem.* **228** (2022) Article ID 113975 (10 pages); <https://doi.org/10.1016/j.ejmech.2021.113975>
 13. B. Mirković, M. Renko, S. Turk, I. Sosič, Z. Jevnikar, N. Obermajer, D. Turk, S. Gobec and J. Kos, Novel mechanism of cathepsin B inhibition by antibiotic nitroxoline and related compounds, *ChemMedChem* **6**(8) (2011) 1351–1356; <https://doi.org/10.1002/cmdc.201100098>
 14. J. S. Shim, Y. Matsui, S. Bhat, B. A. Nacev, J. Xu, H. E. Bhang, S. Dhara, K. C. Han, C. R. Chong, M. G. Pomper, A. So and J. O. Liu, Effect of nitroxoline on angiogenesis and growth of human bladder cancer, *J. Natl. Cancer Inst.* **102**(24) (2010) 1855–1873; <https://doi.org/10.1093/jnci/djq457>
 15. H. Jiang, J. Xing, C. Wang, H. Zhang, L. Yue, X. Wan, W. Chen, H. Ding, Y. Xie, H. Tao, Z. Chen, H. Jiang, K. Chen, S. Chen, M. Zheng, Y. Zhang and C. Luo, Discovery of novel BET inhibitors by drug repurposing of nitroxoline and its analogues, *Org. Biomol. Chem.* **15** (2017) 9352–9361; <https://doi.org/10.1039/c7ob02369c>
 16. W. Chan-On, N. T. B. Huyen, N. Songtawee, W. Suwanjang, S. Prachayasittikul and V. Prachayasittikul, Quinoline-based clioquinol and nitroxoline exhibit anticancer activity

- inducing FoxM1 inhibition in cholangiocarcinoma cells, *Drug Des. Devel. Ther.* **9** (2015) 2033–2047; <https://doi.org/10.2147/DDDT.S79313>
17. J. Lazovic, L. Guo, J. Nakashima, L. Mirsadraei, W. Yong, H. J. Kim, B. Ellingson, H. Wu and W. B. Pope, Nitroxoline induces apoptosis and slows glioma growth in vivo, *Neuro-Oncol.* **17**(1) (2015) 53–62; <https://doi.org/10.1093/neuonc/nou139>
18. H. Mao, Y. Du, Z. Zhang, B. Cao, J. Zhao, H. Zhou and X. Mao X, Nitroxoline shows antimyeloma activity by targeting the TRIM25/ p53 axle, *Anticancer. Drugs* **28**(4) (2017) 376–383; <https://doi.org/10.1097/CAD.0000000000000466>
19. W.-L. Chang, L.-C. Hsu, W.-J. Leu, C.-S. Chen and J.-H. Guh, Repurposing of nitroxoline as a potential anticancer agent against human prostate cancer: A crucial role on AMPK/mTOR signaling pathway and the interplay with Chk2 activation, *Oncotarget* **6** (2015) 39806–39820; <https://doi.org/10.18632/oncotarget.5655>
20. N. Xu, L. Huang, X. Li, M. Watanabe, C. Li, A. Xu, C. Liu, Q. Li, M. Araki, K. Wada, Y. Nasu and P. Huang, The novel combination of nitroxoline and PD-1 blockade, exerts a potent antitumor effect in a mouse model of prostate cancer, *Int. J. Biol. Sci.* **15**(5) (2019) 919–928; <https://doi.org/10.7150/ijbs.32259>
21. J. Kos and A. Mitrović, Nitroxoline: repurposing its antimicrobial to antitumor application, *Acta. Biochim. Pol.* **66**(4) (2019) 521–531; https://doi.org/10.18388/abp.2019_2904
22. H. Wang, Y. Li, F. Sun, Y. Feng, K. Jin and X. Wang, 1,2,3,4-Tetrahydro-8-hydroxyquinoline-promoted copper-catalyzed coupling of nitrogen nucleophiles and aryl bromides, *J. Org. Chem.* **73**(21) (2008) 8639–8642; <https://doi.org/10.1021/jo8015488>
23. F. Yang, F. Song, W. Li, J. Lan and J. You, Palladium-catalyzed C–H activation of anilides at room temperature: Ortho-arylation and acetoxylation, *RSC Adv.* **3** (2013) 9649–9652; <https://doi.org/10.1039/C3RA41981A>

24. O. V. Dolomanov, L. J. Bourhis, R. J. Gildea, J. A. K. Howard and H. Puschmann, OLEX2: A complete structure solution, refinement and analysis program, *J. Appl. Crystallogr.* **42** (2009) 339–341; <https://doi.org/10.1107/S0021889808042726>
25. G. M. Sheldrick, SHELXT – integrated space-group and crystal-structure determination, *Acta Cryst.* **71**(1) (2015) 3–8; <https://doi.org/10.1107/S2053273314026370>
26. C. F. Macrae, I. Sovago, S. J. Cottrell, P. T. A. Galek, P. McCabe, E. Pidcock, M. Platings, G. P. Shields, J. S. Stevens, M. Towler and P. A. Wood, Mercury 4.0: From visualization to analysis, design and prediction, *J. Appl. Cryst.* **53**(1) (2020) 226–235; <https://doi.org/10.1107/S1600576719014092>
27. O. Olaleye, T. R. Raghunand, S. Bhat, C. Chong, P. Gu, J. Zhou, Y. Zhang, W. R. Bishai and J. O. Liu, Characterization of clioquinol and analogues as novel inhibitors of methionine aminopeptidases from *Mycobacterium tuberculosis*, *Tuberculosis* **91**(S1) (2011) S61–65; <https://doi.org/10.1016/j.tube.2011.10.012>
28. R. Kuhelj, M. Dolinar, J. Pungertar and V. Turk, The preparation of catalytically active human cathepsin B from its precursor expressed in *Escherichia coli* in the form of inclusion bodies, *Eur. J. Biochem.* **229**(2) (1995) 533–539; <https://doi.org/10.1111/J.1432-1033.1995.0533K.X>
29. Y. Shimizu, H. Morimoto, M. Zhang and T. Ohshima, Microwave-assisted deacylation of unactivated amides using ammonium-salt-accelerated transamidation, *Angew. Chem. Int. Ed.* **51**(34) (2012) 8564–8567; <https://doi.org/10.1002/anie.201202354>
30. H. Jiang, J. E. Taggart, X. Zhang, D. M. Benbrook, S. E. Lind and W. Q. Ding, Nitroxoline (8-hydroxy-5-nitroquinoline) is more a potent anti-cancer agent than clioquinol (5-chloro-7-iodo-8-quinoline), *Cancer Lett.* **312**(1) (2011) 11–17; <https://doi.org/10.1016/j.canlet.2011.06.032>

31. D. Knez, I. Sosič, A. Pišlar, A. Mitrović, M. Jukič, J. Kos and S. Gobec, Biological evaluation of 8-hydroxyquinolines as multi-target directed ligands for treating Alzheimer's disease, *Curr. Alzheimer Res.* **16**(9) (2019) 801–814; <https://doi.org/10.2174/1567205016666191010130351>
32. W. T. Lowther and B. W. Matthews. Structure and function of the methionine aminopeptidases, *Biochim. Biophys. Acta* **1477**(1-2) (2000) 157–167; [https://doi.org/10.1016/S0167-4838\(99\)00271-X](https://doi.org/10.1016/S0167-4838(99)00271-X)
33. S. Y. Bhat, Drug targeting of aminopeptidases: importance of deploying a right metal cofactor, *Biophys. Rev.* **16** (2024) 249–256; <https://doi.org/10.1007/s12551-024-01192-8>
34. M. A. Altmeyer, A. Marschner, R. Schiffmann and C. D. Klein, Subtype-selectivity of metal-dependent methionine aminopeptidase inhibitors, *Bioorg. Med. Chem. Lett.* **20**(14) (2010) 4038–4044; <https://doi.org/10.1016/j.bmcl.2010.05.093>
35. J. Y. Li, L. L. Chen, Y. M. Cui, Q. L. Luo, J. Li, F. J. Nan and Q. Z. Ye, Specificity for inhibitors of metal-substituted methionine aminopeptidase, *Biochem. Biophys. Res. Commun.* **307**(1) (2003), 172–179; [https://doi.org/10.1016/S0006-291X\(03\)01144-6](https://doi.org/10.1016/S0006-291X(03)01144-6)
36. Q. Z. Ye, S. X. Xie, M. Huang, W. J. Huang, J. P. Lu and Z. Q. Ma, Metalloform-selective inhibitors of Escherichia coli methionine aminopeptidase and X-ray structure of a Mn(II)-form enzyme complexed with an inhibitor, *J. Am. Chem. Soc.* **126**(43) (2004) 13940–13941; <https://doi.org/10.1021/ja045864p>
37. M. Huang, S.-X. Xie, Z.-Q. Ma, Q.-Q. Huang, F.-J. Nan and Q.-Z. Ye, Inhibition of monometalated methionine aminopeptidase: Inhibitor discovery and crystallographic analysis, *J. Med. Chem.* **50**(23) (2007) 5735–5742; <https://doi.org/10.1021/jm700930k>
38. J. Schmitz, E. Gilberg, R. Löser, J. Bajorath, U. Bartz and M. Gütschow, Cathepsin B: Active site mapping with peptidic substrates and inhibitors, *Bioorg. Med. Chem.* (27)11 (2019) 1–15; <https://doi.org/10.1016/j.bmc.2018.10.017>

39. I. Sosič, B. Mirković, K. Arenz, B. Štefane, J. Kos and S. Gobec, Development of new cathepsin B inhibitors: combining bioisosteric replacements and structure-based design to explore the structure–activity relationships of nitroxoline derivatives, *J. Med. Chem.* **56**(2) (2013) 521–533; <https://doi.org/10.1021/jm301544x>
40. A. Mitrović, B. Mirković, I. Sosič, S. Gobec and J. Kos, Inhibition of endopeptidase and exopeptidase activity of cathepsin B impairs extracellular matrix degradation and tumour invasion, *Biol. Chem.* **397**(2) (2016) 165–174; <https://doi.org/10.1515/hsz-2015-0236>
41. L. Sorokin, The impact of the extracellular matrix on inflammation, *Nat. Rev. Immunol.* **10** (2010) 712–723; <https://doi.org/10.1038/nri2852>